

Optimization of Eccentricity during a Two Burn Station Acquisition Sequence of a Geosynchronous Orbit

A project present to
The Faculty of the Department of Aerospace Engineering
San Jose State University

in partial fulfillment of the requirements for the degree
Master of Science in Aerospace Engineering

By

Lynn Chouw

May 2013

approved by

Dr. Periklis Papadopoulos
Faculty Advisor



The Designated Masters Project Committee Approves the Thesis Titled

OPTIMIZATION OF ECCENTRICITY DURING A TWO BURN STATION ACQUISITION
SEQUENCE OF A GEOSYNCHRONOUS ORBIT

by

Lynn Chouw

APPROVED FOR THE AEROSPACE ENGINEERING PROGRAM

SAN JOSÉ STATE UNIVERSITY

May 2013

Dr. Periklis Papadopoulos

Aerospace Engineering

Dr. Sean Swei

NASA Ames Research Center

Mary Johnson

NASA Ames Research Center

ABSTRACT

OPTIMIZATION OF ECCENTRICITY DURING A TWO BURN STATION ACQUISITION SEQUENCE

By Lynn Chouw

Optimization of orbit transfers to reach geosynchronous orbit is an old problem with many solutions. This paper documents the attempt to numerically solve the problem while keeping a target eccentricity as the priority. An algorithm is introduced that accepts inputs of an initial orbit, a burn time and a desired longitude and outputs an optimal ratio of the two burns to achieve the desired eccentricity in the orbit.

ACKNOWLEDGEMENTS

I would like to thank my family for supporting me through my journey in higher education. I would not have been able to complete anything without their love and encouragement.

I would also like to thank Dr. Periklis Papadopoulos and Dr. Nikos Mourtos for their academic guidance as I was completely lost when the Lockheed Martin/San Jose State University Cohort program was cancelled.

Finally, I would like to thank my committee members for their expertise and time to help me complete this project.

Table of Contents

List of Tables.....	6
List of Figures.....	6
Nomenclature.....	7
1 Introduction.....	8
2 Methodology.....	9
3 Results.....	13
4 Conclusion.....	27
5 References.....	29
Appendix A.....	30
Appendix B.....	31

List of Tabl

Table 1: Run A: Eccentricity Varying First Burn Start Time.....	24
Table 2: Run B: Eccentricity Varying First Burn Start Time.....	26

List of FiguresY

Figure 1: Final Eccentricity Varying Burn 1 and Burn 2.....	13
Figure 2: Final Drift Varying Burn 1 and Burn 2.....	14
Figure 3: Optimal Burn Drift Profile.....	15
Figure 4: Optimal Burn Eccentricity Profile.....	16
Figure 5: Optimal Burn Drift Profile Targeting Longitude.....	17
Figure 6: Optimal Burn Eccentricity Profile Targeting Longitude.....	18
Figure 7: Optimal Burn Longitude Plot.....	19
Figure 8: Optimal Burn Longitude and Drift Rate Plot.....	20
Figure 9: Run A: Final Eccentricity Varying Burn 2 Start Times.....	21
Figure 10: Run A: Burn Ratio Varying Burn 2 Start Times.....	22
Figure 11: Run A: Burn Ratio Varying Start Times.....	23
Figure 12: Run A: Final Eccentricity Varying Start Times.....	24
Figure 13: Run B: Burn Ratio Varying Start Times.....	25
Figure 14: Run B: Final Eccentricity Varying Start Times.....	26

Nomenclature

A	Unperturbed geostationary semimajor axis = 42164.2 km
a	Orbit semimajor axis
D	Drift rate
e	Orbit eccentricity
ECF	Earth Centered Fixed
ECI	Earth Centered Inertial
GAST	Greenwich Apparent Sidereal Time
GMST	Greenwich Mean Sidereal Time
i	inclination
p	Semi-latus rectum
\mathbf{r}	Position vector of the satellite
r	Magnitude of the position vector of the satellite
$\dot{\mathbf{r}}$	Acceleration vector
raan	Right ascension of the ascending node
\mathbf{V}	Velocity vector
V	Magnitude of velocity vector
ω	Argument of perigee
v	True anomaly
x	x component of position vector
y	y component of position vector
z	z component of position vector

Δ Instantaneous change of a variable

δ difference of a variable

μ Gravity potential of Earth = 398600.4418 $\frac{km^3}{s^2}$

1 Introduction

Orbital maneuvers have been studied for a long time. Hohmann solved the problem of transfers between two coplanar circular orbits with a minimum velocity applied to the space vehicle (Hohmann, 1925). The problem of two impulse orbit maneuvers has been studied over the years with minor tweaks in order to apply solutions to real spacecraft. Jezewski and Mittleman (1982) wrote about an analytical approach to two fixed impulse transfers, while Jin and Melton (1991) concluded that using two impulsive maneuvers of fixed magnitudes is only possible for certain thrust directions.

In the current age of affordability in the Aerospace industry, optimization problems are becoming increasingly important. As a satellite nears completion of orbit transfer, plans must be made in order to place the satellite into its final orbit. Geostationary satellites are equipped with thrusters that allow the satellite to be commanded to maneuver the spacecraft into the desired orbit. These burns are usually tangential to the orbit plane or orthogonal to the orbit plane. Tangential burns are also known as along-track burns, and changes the longitude of the satellite. This affects the semimajor axis, the longitude drift rate and the eccentricity vector. Orthogonal burns change the orientation of the orbit plane. This includes the inclination and the ascending node. (Soop, 2010).

This paper deals only with tangential burns in line with the orbit plane. In order to “stop” at the final station location in geosynchronous orbit, the satellite needs to have a semimajor axis of 42164.2 km, a drift rate of zero, and an eccentricity vector very close to zero.

It is usually optimal to command orbit maneuvers during the apsides of the orbit (Sgubini, & Teofilatto, 2002), but with affordability being a main driver, for the sake of time, orbit maneuvers are sometimes scheduled at non-optimal times. The time of the maneuver can be

varied to change the eccentricity vector direction, however, with this being set by limitations of time, having multiple burns enables some variability in the final eccentricity of the orbit. This paper will deal with two burns separated by 12 hours. This first objective of this work is to identify the sizes of these two burns for a specific orbit that will give the result of a final eccentricity as close as possible to the target eccentricity. The second objective is to find any general conclusions between the burn sizes and eccentricity that can be used on general orbits.

2 Methodology

The investigation was done by varying the ratio of the two burns and propagating through an ephemeris at a specified burn time, using Matlab as the computing tool. The orbit was modeled using the two body model equations with no perturbations. The input sheet includes the ephemeris in classical orbit parameters, which are then rotated into Earth Centered Inertial (ECI) coordinates for propagation using the equations 1-4 (Wertz & Larson, 1999).

Equation 1

$$p = a * (1 - e^2)$$

Equation 2

$$r = \frac{p}{(1 + e * \cos \square)}$$

Equation 3

$$\begin{aligned}
 & \omega + \dot{\iota} \\
 & \dot{\iota} \\
 & \omega + \dot{\iota} \\
 & \dot{\iota} \\
 & \dot{\iota} \\
 & (\dot{\iota} \dot{\iota} \dot{\iota} \dot{\iota}) \\
 & \omega + \dot{\iota} \\
 & \dot{\iota} \\
 & \omega + \dot{\iota} \\
 & \dot{\iota} \\
 & \dot{\iota} \\
 & (\dot{\iota} \dot{\iota} \dot{\iota} \dot{\iota}) \\
 & \omega + \dot{\iota} \\
 & \dot{\iota} \\
 & (\dot{\iota} \dot{\iota}) \\
 & i * \sin \dot{\iota} r * \sin i * \sin \dot{\iota} \\
 & \dot{\iota} \cos \dot{\iota} \\
 & + \cos(\text{raan}) \dot{\iota} \\
 & \dot{\iota} \\
 & \cos \dot{\iota} \\
 & i * \sin \dot{\iota} r * \dot{\iota} \\
 & (\text{raan}) * \cos \dot{\iota} \\
 & (\text{raan}) - \sin \dot{\iota} \\
 & \dot{\iota} \\
 & \cos \dot{\iota} \\
 & \dot{\iota} \\
 & r * \dot{\iota} \\
 & r = \begin{bmatrix} x \\ y \\ z \end{bmatrix} = \dot{\iota}
 \end{aligned}$$

Equation 4

$$\begin{aligned}
 & \omega + \dot{\omega} \\
 & \omega + \dot{\omega} \\
 & (\dot{\omega} + e \cdot \cos \omega) \\
 & \cos \dot{\omega} \\
 & \dot{\omega} \\
 & \omega + \dot{\omega} \\
 & \omega + \dot{\omega} \\
 & (\dot{\omega} + e \cdot \cos \omega) \\
 & \cos \dot{\omega} \\
 & \dot{\omega} \\
 & \omega + \dot{\omega} \\
 & \cos(\dot{\omega} + e \cdot \cos \omega) \\
 & i \cdot (\dot{\omega}) \\
 & (\dot{\omega} + e \cdot \sin \omega) - \cos \text{raan} \cdot \cos i \cdot \dot{\omega} \\
 & \sin \dot{\omega} \\
 & \sin \text{raan} \cdot \dot{\omega} \\
 & (\dot{\omega} + e \cdot \sin \omega) + \sin \text{raan} \cdot \cos i \cdot \dot{\omega} \\
 & \sin \dot{\omega} \\
 & \cos \text{raan} \cdot \dot{\omega} \\
 & \dot{\omega} \\
 & -\sqrt{\frac{\mu}{p}} \cdot \dot{\omega} \\
 V = \begin{bmatrix} \delta x \\ \delta y \\ \delta z \end{bmatrix} = \dot{\omega}
 \end{aligned}$$

The vector can be propagated forward in time by multiplying a time step with the velocity and acceleration found from equation 5 (Vallado, 2007).

Equation 5

$$\dot{r} + \frac{\mu}{a^3} r = 0$$

The initial drift rate of the orbit, or how quickly the orbit is rotating with respect to the rotation of the earth, is given by equation 6 (Soop, 2010). To find the thrust needed to reduce the drift rate to zero, Soop (2010) provides equation 7.

Equation 6

$$D = \frac{-1.5 \cdot \delta a}{A}$$

Equation 7

$$\Delta D = \frac{-3\Delta V}{V}$$

Using the ΔV , an array is created by splitting the value between the two burns by a percentage. In this simulation, one percent was the step change between each case. A custom Runge Kutta algorithm was written in order to propagate the ephemeris while controlling the time steps. In the simulation a time step of 60 seconds was used. The Runge Kutta algorithm also checked to see if the burn time was passed during the calculation step, and if it was, inserted an instantaneous thrust or dV at that time.

In order to see if the space vehicle ends up at the correct station, longitude also needed to be calculated. Although the ephemeris is already calculated in ECI, this needs to be converted to an Earth Centered Fixed (ECF) coordinate system. Since longitude is only based on the position, we only need to convert the position vector from ECI to ECF, given by Eagle (n.d.) in equation 8 and 9.

Equation 8

$$r_{ecf} = [T]r_{eci}$$

Equation 9

$$[T] = \begin{bmatrix} \cos \theta & \sin \theta & 0 \\ -\sin \theta & \cos \theta & 0 \\ 0 & 0 & 1 \end{bmatrix}$$

where θ is equal to the Greenwich sidereal time at the moment. This can be calculated from the current day and time by first calculating the Julian Date using Equation 10 (Vallado,2007), then by finding Greenwich Mean Sidereal Time (GMST) by using equation 11 and 12 (Vallado, 2007).

Equation 10

$$JD = 367 * year - \int \left\{ \frac{7 \left\{ year + \int \left(\frac{month+9}{12} \right) \right\} \right\}}{4} \right\} + \int \left(\frac{275 month}{9} \right) + day + 1721013.5 + \frac{\left(\frac{second}{60} + minute \right)}{60} + hour$$

Equation 11

$$T_{UT1} = \frac{JD - 2451545.0}{36525}$$

Equation 12

$$\theta_{GMST} = 67310.54841 (876600 * 3600 + 8640184.812866) T_{UT1} + 0.093104 T_{UT1}^2 - 6.2 e^{-6} T_{UT1}^3$$

GMST is then converted to Greenwich Apparent Sidereal Time (GAST) by using the following equation (Eagle, n.d).

Equation 13

$$\begin{aligned} & \varepsilon_m + \Delta \varepsilon \\ \theta_{GMST} + \Delta \varphi \cos(i, 360) \\ \theta_{GAST} = \text{mod } i \end{aligned}$$

$\Delta \varphi$ is the nutation in longitude, ε_m is the mean obliquity of the ecliptic and $\Delta \varepsilon$ is the nutation in obliquity. The mean obliquity of the ecliptic can be determined from the following equation from Vallado (2007).

Equation 14

$$\varepsilon_m = 23.439291 - 0.0130042 * T_{UT1} - 1.64 * 10^{-7} T_{UT1}^2 + 5.04 * 10^{-7} T_{UT1}^3$$

The nutations in obliquity and longitude involve the following three trigonometric arguments (Eagle, n.d.)

Equation 15

$$L = 280.4665 + 36000.7698 T_{UT1}$$

Equation 16

$$L' = 218.3165 + 481267.8813 T$$

Equation 17

$$\Omega = 125.04452 - 1934.136261 T$$

The equations for nutation in longitude and nutation in obliquity using the trigonometric arguments are listed below in arc seconds (Eagle, n.d.).

Equation 18

$$\Delta \varphi = -17.20 \sin \Omega - 1.32 \sin 2L - .23 \sin 2L' + 0.21 \sin 2\Omega$$

Equation 19

$$\Delta \varepsilon = 9.20 \cos \Omega + 0.57 \cos 2L + 0.10 \cos 2L' - 0.09 \cos 2\Omega$$

After converting the results from equations 18 and 19 into degrees and putting them along with the result from equation 14 into equation 13 the Greenwich Apparent Sidereal Time in degrees is obtained. This can be put back into equation 9 which will create the matrix to convert the position ECI vector into the position ECF vector.

Wertz and Larson (1999) provide the equation to calculate longitude from the ECF vector.

Equation 20

$$\lambda = \tan^{-1} \frac{y}{x}$$

The longitude value is calculated at every step of the Runge Kutta and at the end of the script the burn parameters with the longitude closest to the desired longitude is selected.

3 Results

For this simulation, an orbit and a burn time were randomly selected. A starting drift rate of 1 deg/day (eastward) was selected as this seems to be reasonable for current satellites. The input file can be seen in Appendix A. These results do not target a specific longitude.

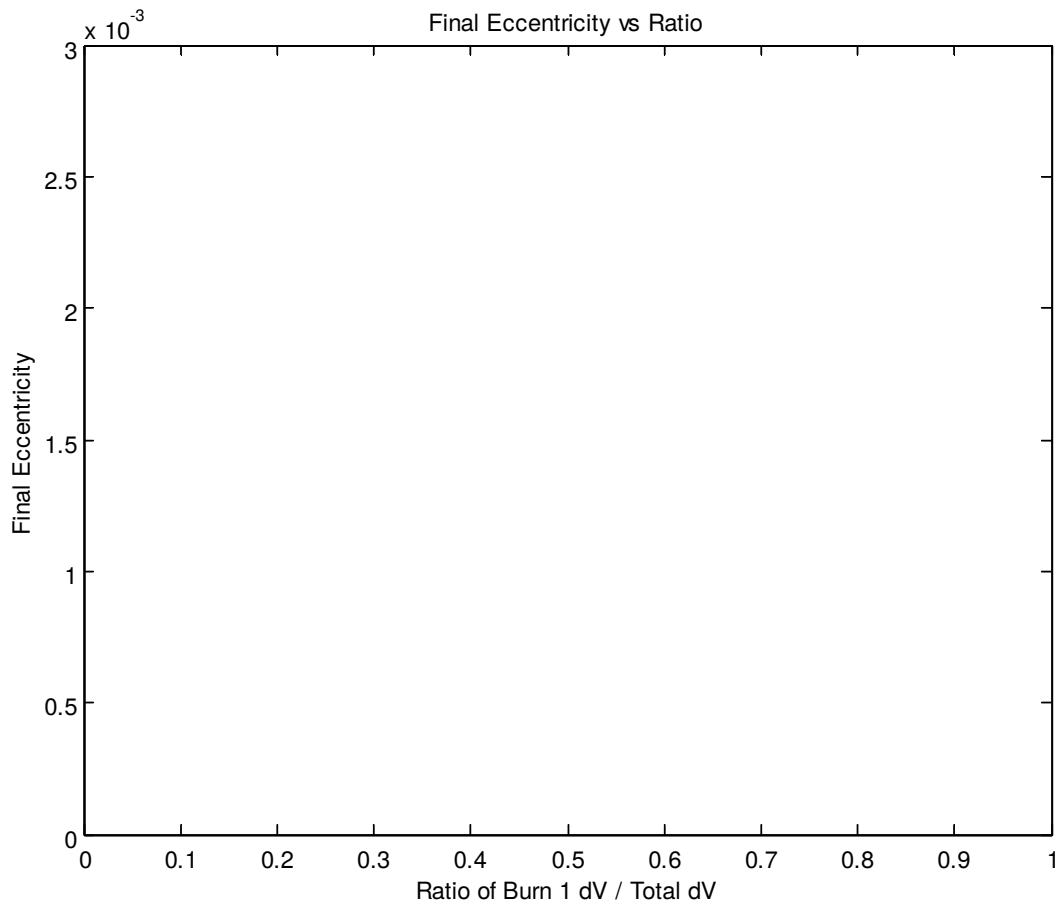


Figure 1: Final Eccentricity Varying Burn 1 and Burn 2

Figure 1 shows the final eccentricity did have a minimum Rvalue at a ratio of 75% dV for burn 1 and 25% of the dV for burn 2. It is a good check that at 50%, the eccentricity is about the same as the initial eccentricity. Two dV burns of equal size on opposite sides of the orbit should cancel each other out.

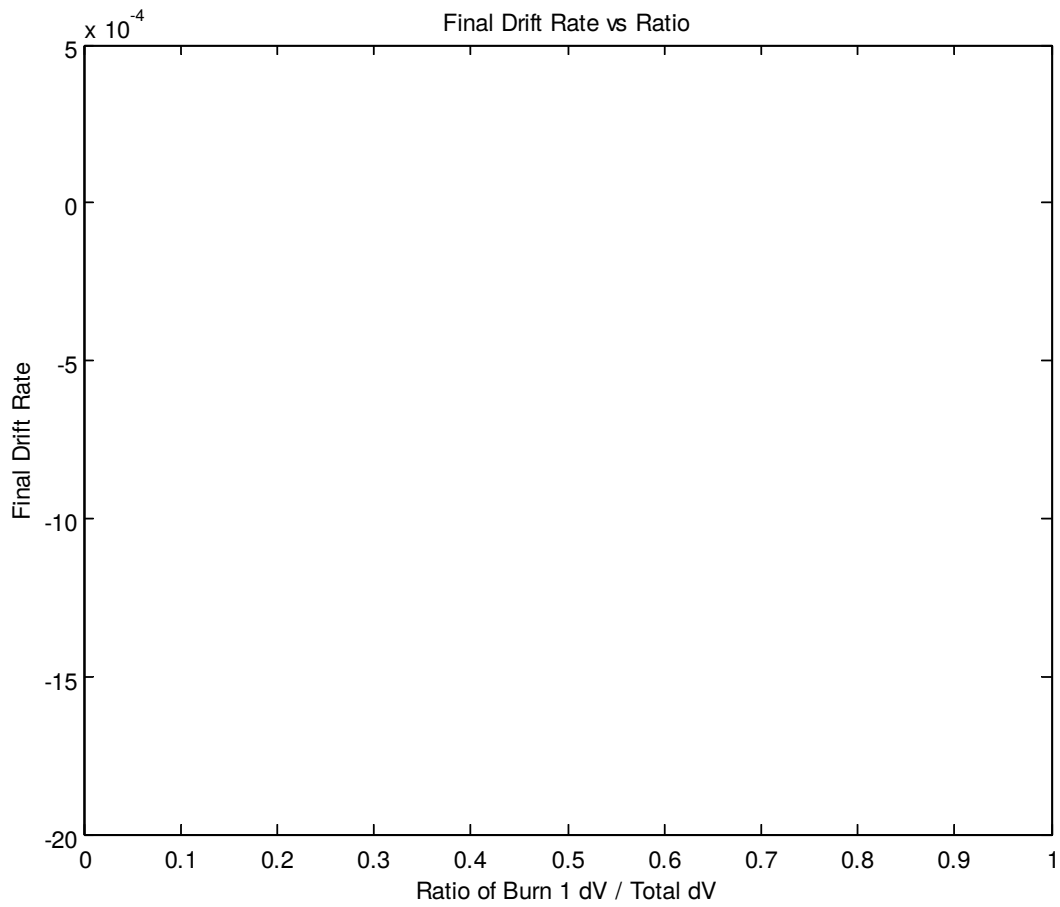


Figure 2: Final Drift Varying Burn 1 and Burn 2

While the difference between the two extremes is not large, it is interesting to note that Figure 2 indicates that more drift rate is taken out of the orbit when the first burn is larger. This could be related to the 12 hours between the burns. For a large first burn, this would leave the 12 hour waiting period at a lower drift rate.

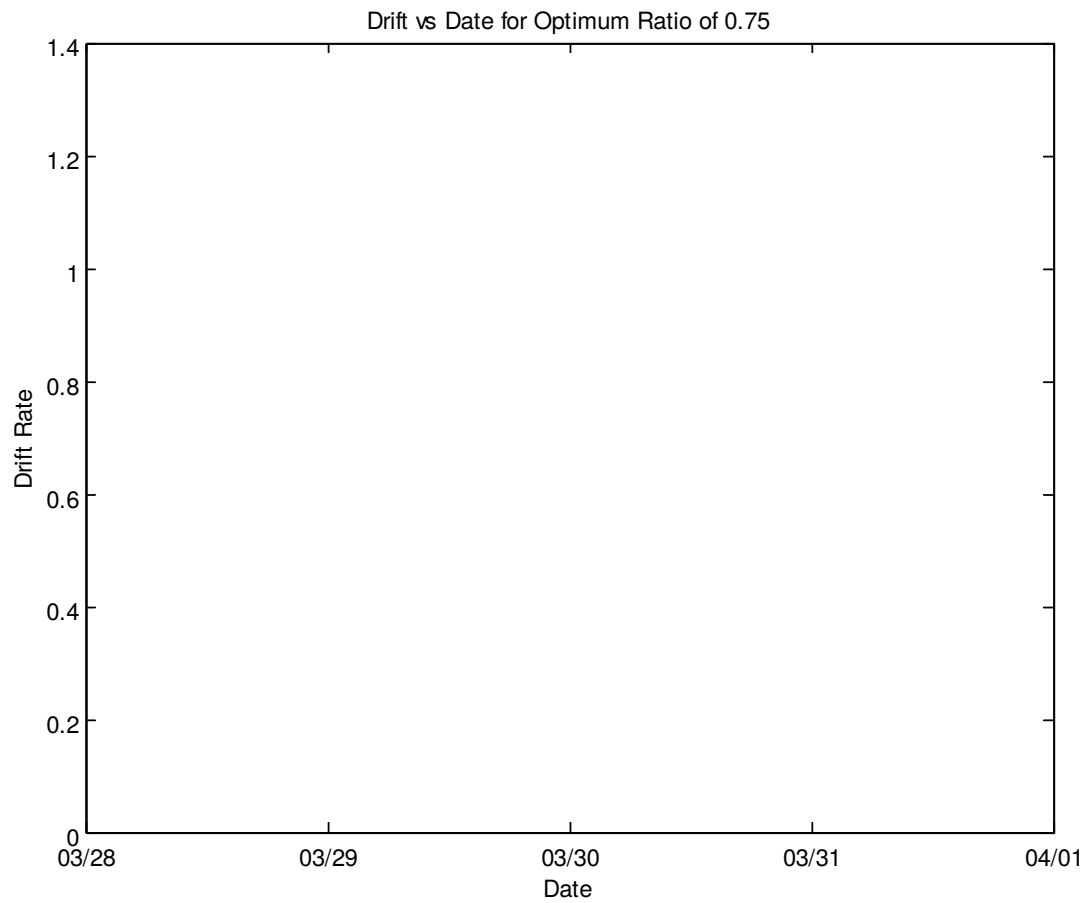


Figure 3: Optimal Burn Drift Profile

Figure 3 shows the drift profile for the optimal ratio, in this case 75% burn one and 25% burn two. The burns affect the orbit as expected, removing 75% of the drift rate during burn one and 25% of the drift rate during burn two.

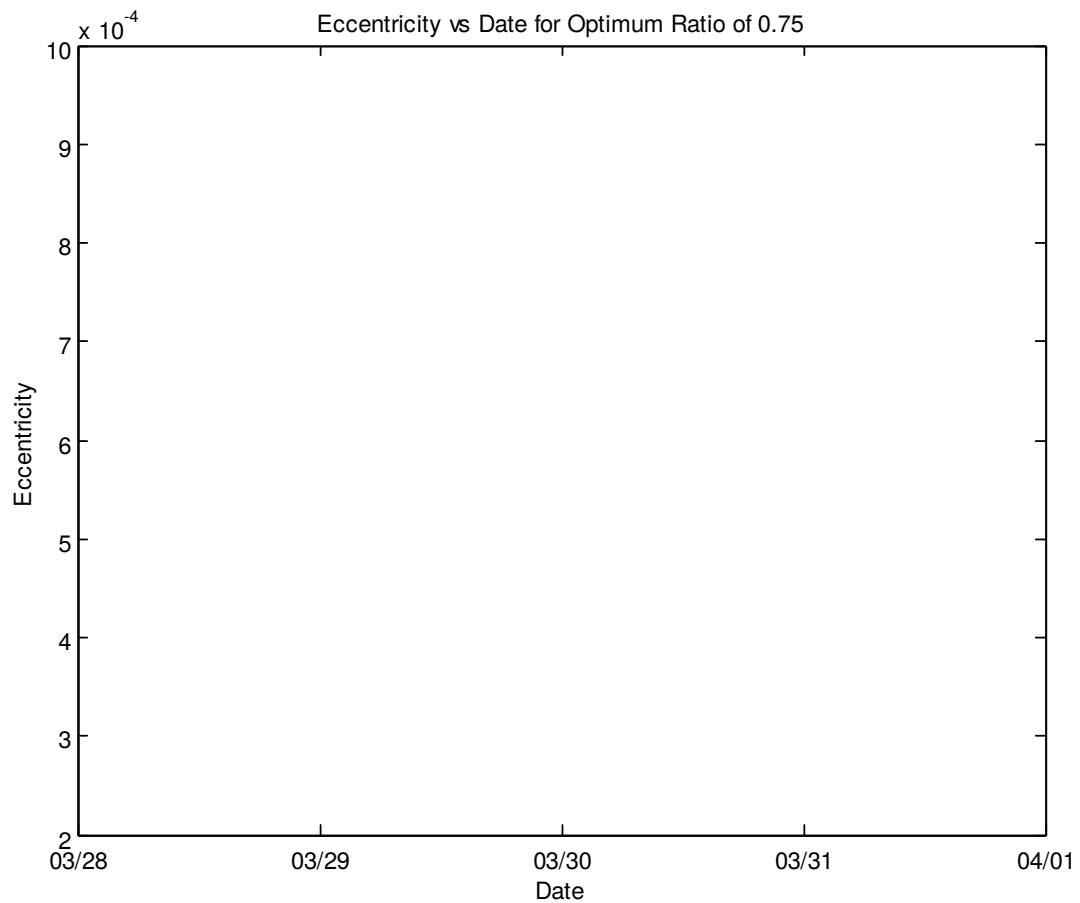


Figure 4: Optimal Burn Eccentricity Profile

The eccentricity profile shown in Figure 4 is from the same optimal burn ratio. Although the first burn accounts for 75% of the total dV, it only takes out 72% of the total eccentricity change.

Figures 1-4 show the results of the simulation if longitude is not targeted. By targeting a longitude, the results change drastically. Instead of optimizing for only eccentricity, for each ratio percentage change, the script finds the solution that results in the closest desired longitude. That case with the desired longitude will have an eccentricity associated with it which may or may not correspond to the lowest eccentricity for a general case.

Using the same inputs as Figures 1-4, the script was run again but targeting a longitude of 121 degrees. Figures 1 and 2 are still the same as it shows the final eccentricity and drift for a varying ratio.

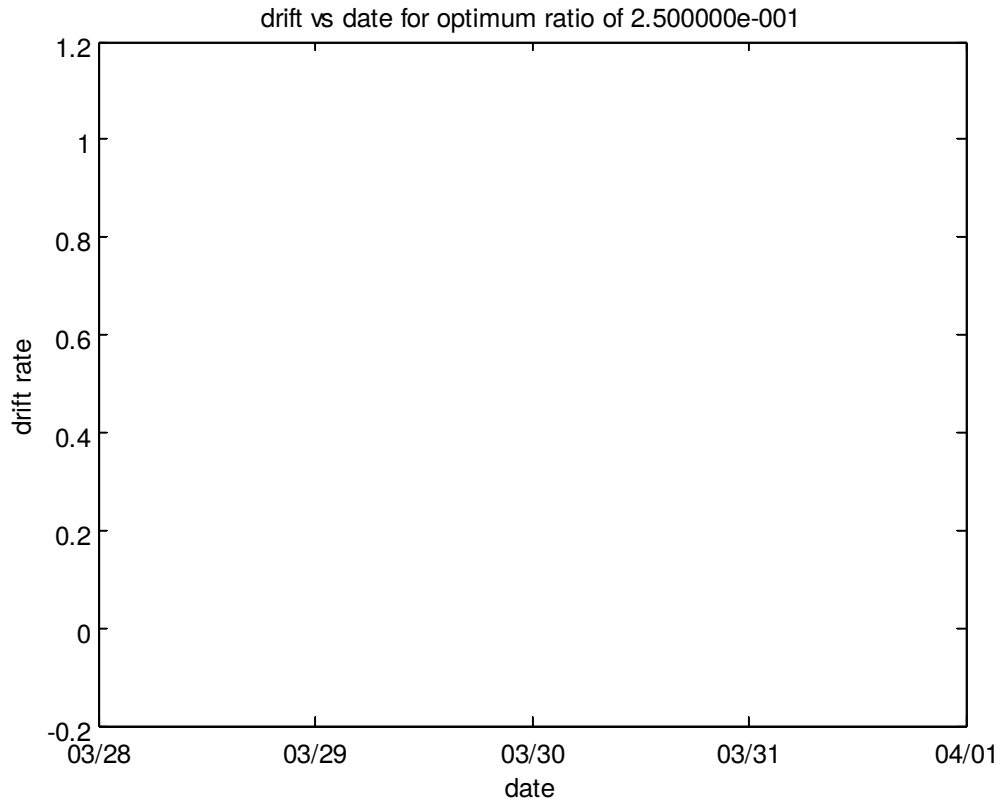


Figure 5: Optimal Burn Drift Profile Targeting Longitude

In comparison to Figure 3, Figure 5 shows an optimal ratio of 25. This is very different from the ratio of 75 for Figure 3, however both still result in a drift rate close to zero.

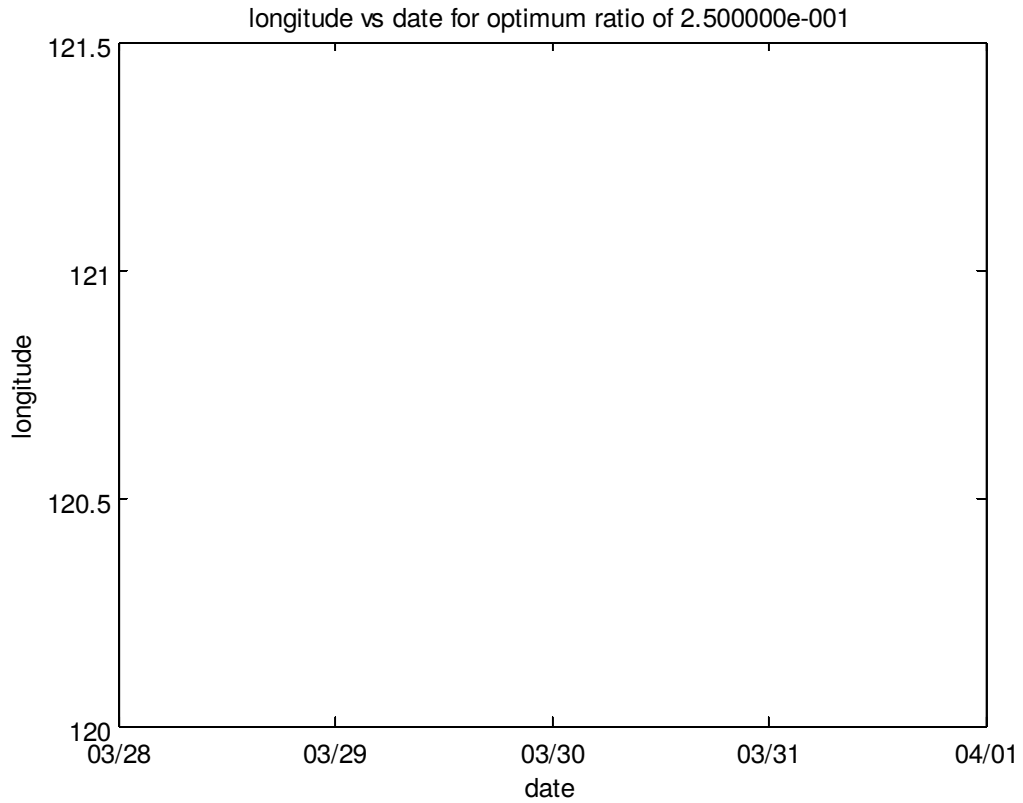


Figure 7: Optimal Burn Longitude Plot

Figure 7 shows the resulting longitude with time. The wide oscillations in longitude indicate that the longitude is an instantaneous longitude. The simulation searches for a longitude at the end of the plot close to the desired longitude.

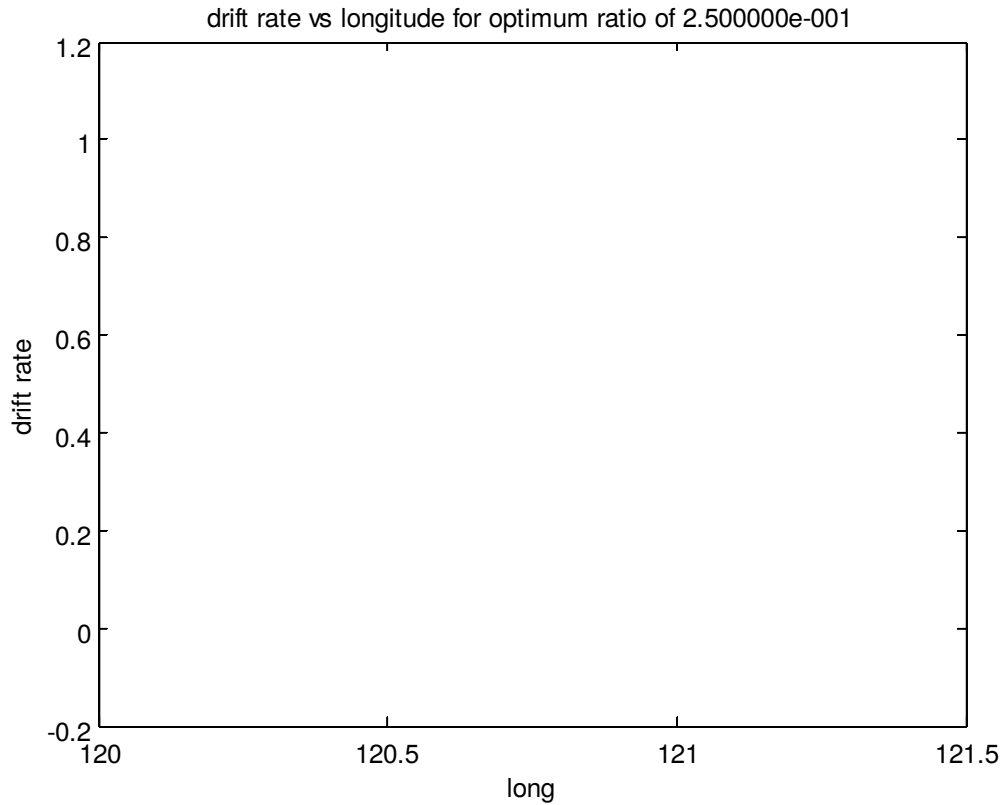


Figure 8: Optimal Burn Longitude and Drift Rate Plot

Figure 8 shows how drift rate varies with longitude. The burns can be seen as the long straight vertical lines. The reason why the longitude is a long horizontal line for a specific drift rate is because of the changing instantaneous longitude that can be seen in Figure 7.

In order to change the eccentricity to a lower value while still targeting longitude, the simulation was run while varying the first burn start time by one hour increments. In addition, as part of the simulation the second burn time was varied from the nominal burn time of 12 hours after the first burn. Figures 9 and 10 show an example of the plot of varying the burn time of the

second burn and its result for burn ratio and eccentricity.

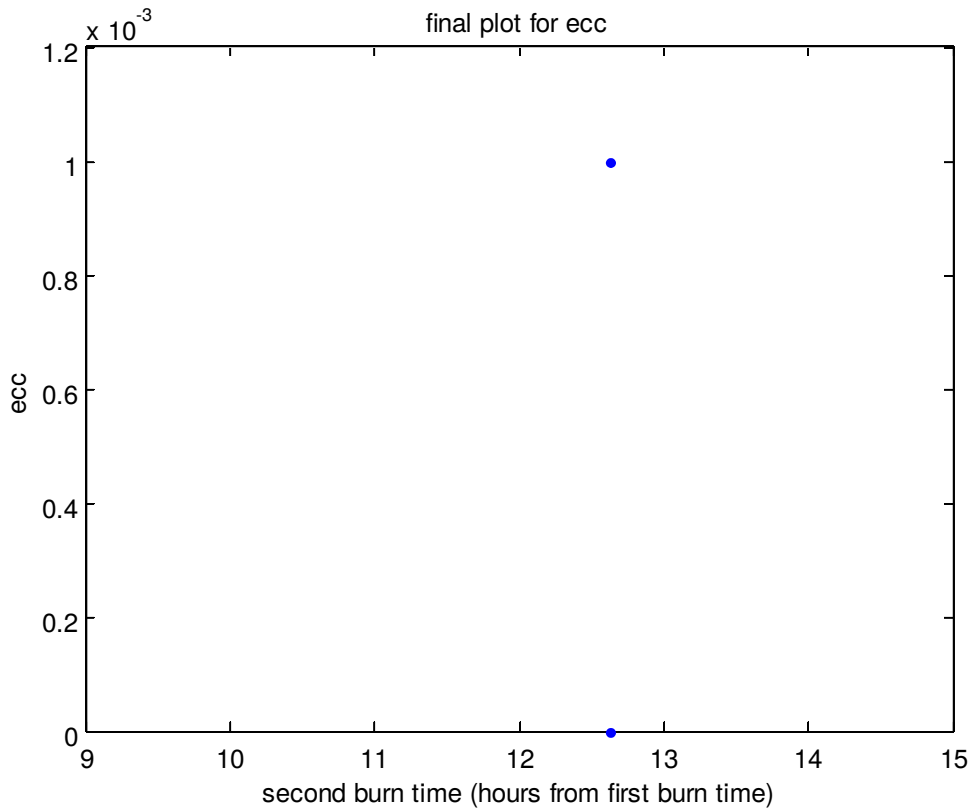


Figure 9: Run A: Final Eccentricity Varying Burn 2 Start Times

The vertical line in the plot represents apogee time. While the eccentricity at 12 hours after the first burn is 0.0007, which is smaller than the original eccentricity value of 0.0009, there is still some potential for a smaller eccentricity merely by delaying the second burn to 13 hours after the first burn instead of 12 hours after the first burn.

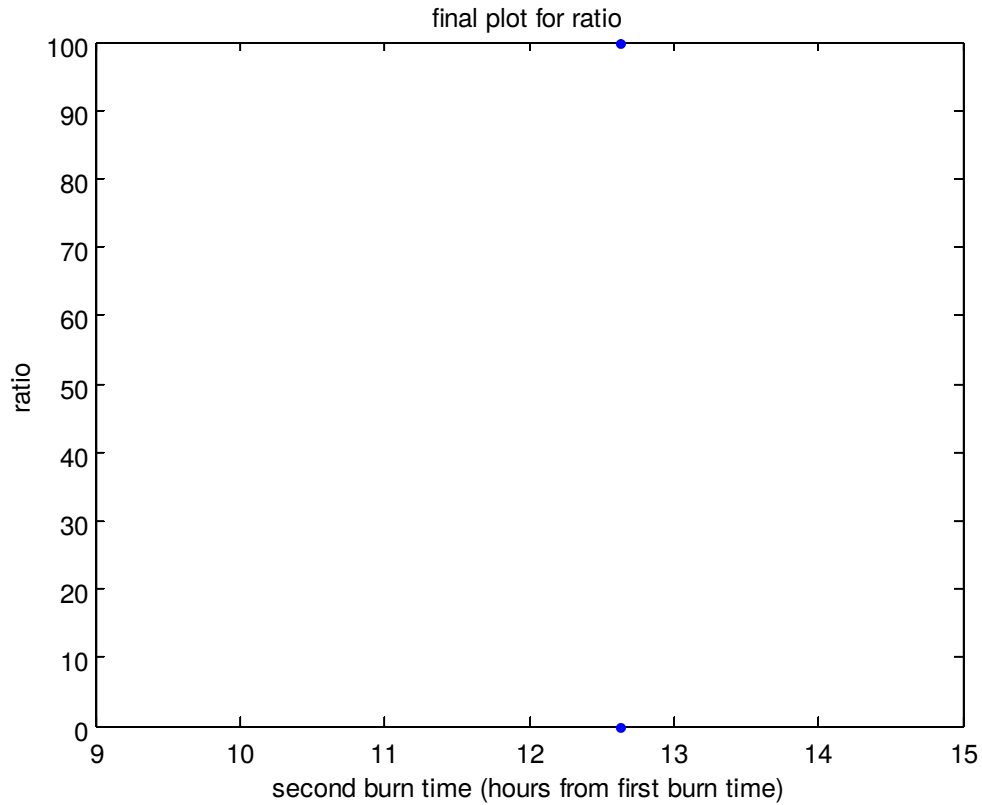


Figure 10: Run A: Burn Ratio Varying Burn 2 Start Times

As shown in Figure 10, the burn ratio does not vary much when changing the start time of the second burn.

In order to find the optimal time for the start of the first burn, Figures 9 and 10 were produced for multiple start times at one hour increments. The results are summarized in Figures 11 and 12.

Run A: Ratio vs Burn 1 Start Time

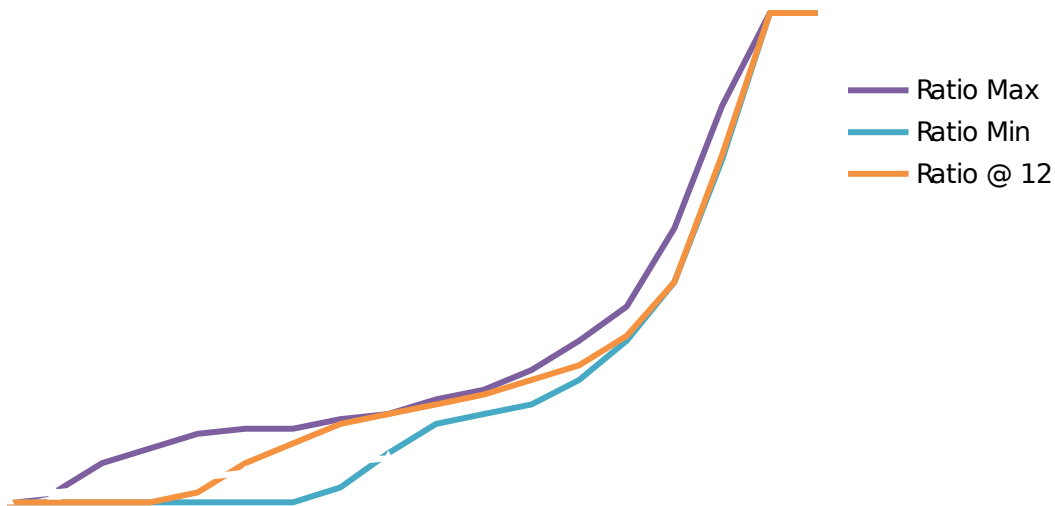


Figure 11: Run A: Burn Ratio Varying Start Times

Ratio @ 12 plots the optimal ratio for the first burn shown by the horizontal axis and the second burn 12 hours later. Ratio Min and Max show the minimum and maximum optimal ratios when varying the start time of the second burn by three hours.

There is a limit on both extremes. The values all go to zero when the burns start too early. Since the simulation calculates an optimal dV based on one impulse, if the burn starts when the initial longitude is too far away there is no way that the dV will be able to achieve the desired longitude with any burn ratio. Likewise if the first burn starts too late, there is no time for a second burn and the burn ratio is always 100%.

Run A: Ecc vs Burn 1 Start Time

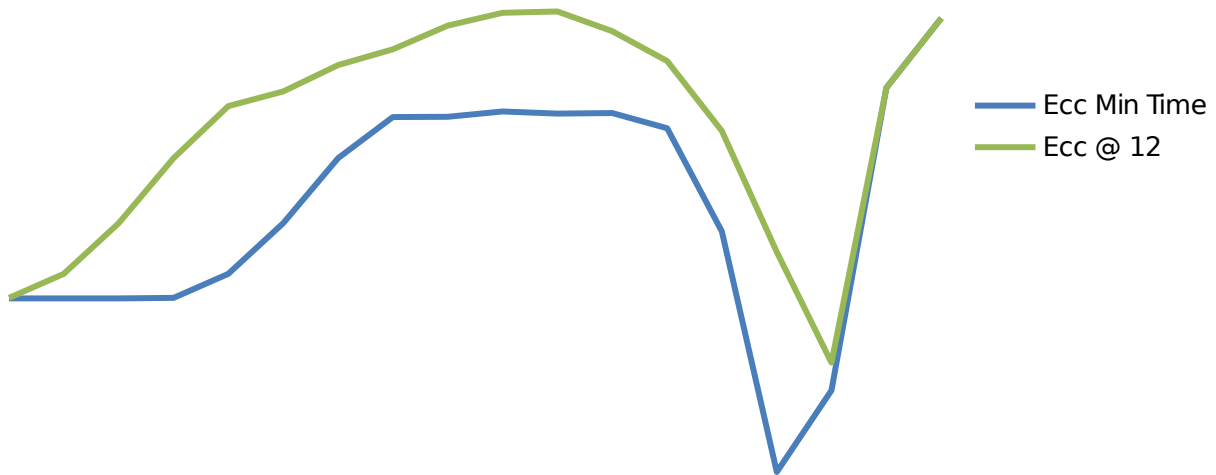


Figure 12: Run A: Final Eccentricity Varying Start Times

Similar to the Burn Ratio plot shown in Figure 9, Ecc @ 12 plots the final eccentricity for the first burn shown by the horizontal axis and the second burn 12 hours later. Ecc Min Time shows the minimum final eccentricity when varying the start time of the second burn by three hours.

Ecc @ 12 is consistently larger than the minimum eccentricity except near the end of the data. Table 1 shows the breakdown of the time of the minimum eccentricity.

Table 1: Run A: Eccentricity Varying First Burn Start Time

Date/Time	Ecc Min	Ecc Min Time	Ecc @ 12
3/28/12 13:00	0.000924 4	11.75	0.0009261
3/28/12 14:00	0.000924 4	10.75	0.001009
3/28/12 15:00	0.000924 4	9.75	0.001185
3/28/12 16:00	0.000926 1	9	0.001411
3/28/12 17:00	0.001009	9	0.001591
3/28/12 18:00	0.001185	9	0.001642
3/28/12 19:00	0.001411	9	0.001733
3/28/12 20:00	0.001553	9	0.001788
3/28/12 21:00	0.001554	9	0.00187
3/28/12 22:00	0.001572	9	0.001914
3/28/12 23:00	0.001565	9	0.001919
3/29/12 0:00	0.001567	9	0.001851
3/29/12 1:00	0.001514	9	0.001747
3/29/12 2:00	0.001156	15	0.001505
3/29/12 3:00	0.000322 4	15	0.001085
3/29/12 4:00	0.000605 4	13.25	0.000701
3/29/12 5:00	0.001655	12	0.001655
3/29/12 6:00	0.001896	12	0.001896

Note that the time of the minimum eccentricity starts around 12, goes to the lower limit, jumps to the upper limit then returns to something around 12. These correspond to the extremes seen in Figure 11 at burn ratios of 0 and 100%.

Additional studies were done with the input values shown in Appendix B. The summary plots of varying the first burn are shown in Figures 13 and 14.

Run B: Ratio vs Burn 1 Start Time

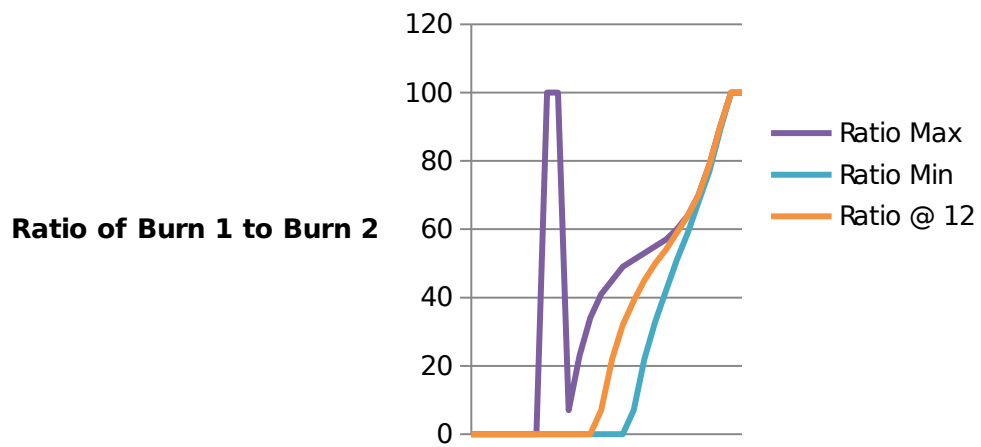


Figure 13: Run B: Burn Ratio Varying Start Times

Figure 13 is odd in that it has a couple 100% ratio maximums near the beginning. This is due to extremely unlucky instantaneous longitude calculations for that time.

Run B: Ratio vs Burn 1 Start Time

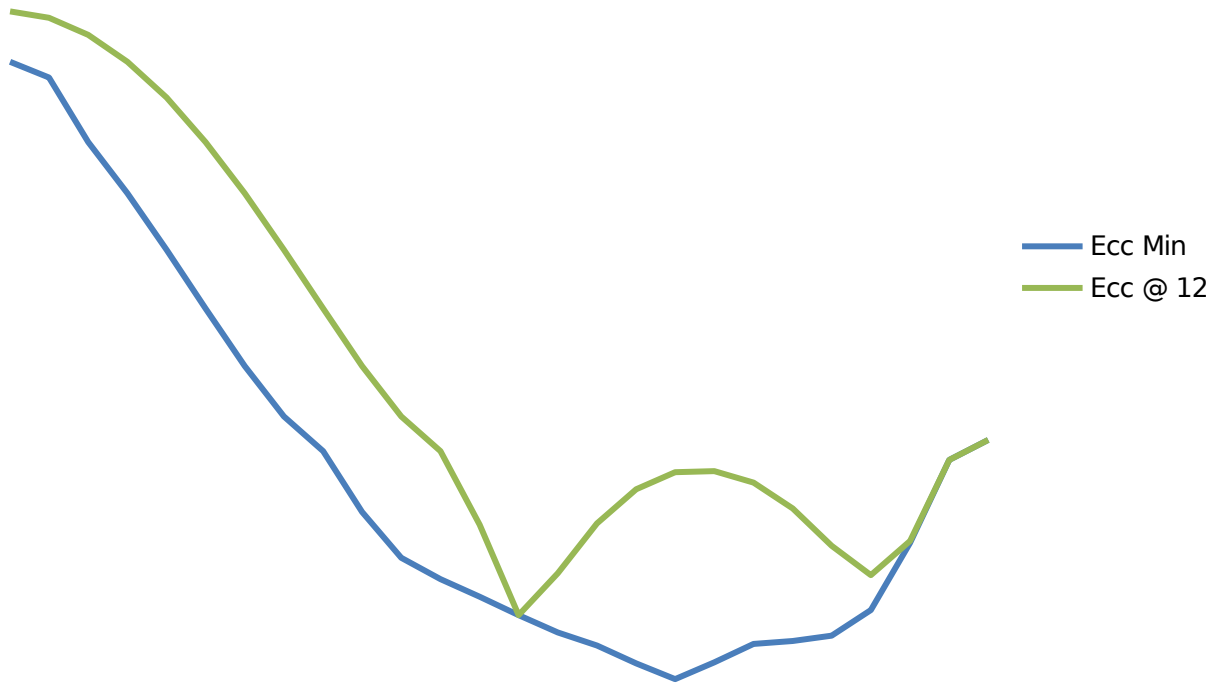


Figure 14: Run B: Final Eccentricity Varying Start Times

There is an interesting jump in the eccentricity between 1:00 and 10:00 start time. It seems as if it should follow the general shape of the eccentricity minimum curve. However, the jump occurs when the ratio for 12 hours after the burn becomes non-zero.

Table 2: Run B: Eccentricity Varying First Burn Start Time

Date/Time	Ecc Min	Ecc Min Time	Ecc @ 12
4/27/13 12:00	0.00255 3	15	0.002755
4/27/13 13:00	0.00249	15	0.002729
4/27/13 14:00	0.00223 1	15	0.002661
4/27/13 15:00	0.00202 6	15	0.002553
4/27/13 16:00	0.0018	15	0.002409
4/27/13 17:00	0.00156 5	15	0.002231
4/27/13 18:00	0.00133 4	15	0.002026
4/27/13 19:00	0.00113 2	15	0.0018
4/27/13 20:00	0.00099 36	15	0.001565
4/27/13 21:00	0.00075 03	15	0.001334
4/27/13 22:00	0.00056 62	14.5	0.001132
4/27/13 23:00	0.00048 13	13.75	0.0009936
4/28/13 0:00	0.00041 07	12.75	0.0006988
4/28/13 1:00	0.00033 72	12	0.0003372
4/28/13 2:00	0.00026 76	11.25	0.0005048
4/28/13 3:00	0.00021 53	10.5	0.0007044
4/28/13 4:00	0.00014 37	9.75	0.0008412
4/28/13 5:00	8.07E- 05	9	0.0009093
4/28/13 6:00	0.00014 75	9	0.0009139
4/28/13 7:00	0.00022 13	9	0.0008671
4/28/13 8:00	0.00023 28	9	0.0007642
4/28/13 9:00	0.00025 46	9	0.0006145
4/28/13 10:00	0.00035	9.75	0.0004972

	75		
4/28/13 11:00	0.00062 67	11.25	0.0006334
4/28/13 12:00	0.00095 8	12	0.000958
4/28/13 13:00	0.00103 8	12	0.001038

Like in Run A, the eccentricity is at a minimum near when the burn ratio is 0% and the time between the burns is high. The optimum time between burns also decreases as the burn ratio gets higher.

4 Conclusion

Given an initial orbit and burn time, this simulation successfully answers the question of what size two burns 12 hours apart should be in order to get a minimum eccentricity value while targeting a specific longitude. In addition, the simulation can vary the separation time between the two burns in order to further minimize the eccentricity value.

While this simulation does answer the specific question of the optimal burn percentage split for a particular orbit, it is very specific to each case. A general conclusion that can be made is that if the dV needed to get zero degrees drift rate is too small, no amount of varying the burns can result in smaller eccentricity or in achieving the desired longitude.

In future studies, the most meaningful update would to change the longitude from instantaneous longitude to a mean longitude. This would make the targeting more meaningful and get rid of any erroneous conclusions based on the varying instantaneous longitude. It would be interesting to modify the simulation to target not only a minimum eccentricity value, but to also target the eccentricity vector direction. Specifically, due to thermal constraints, many satellites try to follow the sun vector and it would be beneficial if this simulation could setup the

satellite to point in the correct direction. Also, as satellites reach their final geosynchronous orbit, they start to keep track of time in terms of the satellite's position and the sun's position. This allows spacecraft operators to keep track of when the satellite will be subject to thermal constraints. Adding this time system to the simulation will make it easier for users to calculate burn times.

5 References

- Eagle, C.D. (n.d.). Astrodynamic coordinates. *Orbital mechanics with Numerit Pro*. Retrieved March 14, 2013, from <http://www.cdeagle.com>
- Eagle, C.D. (n.d.). Greenwich apparent sidereal time. *Celestial computing with Numerit Pro*. Retrieved March 14, 2013, from <http://www.cdeagle.com>
- Hohmann, W. (1925). The attainability of heavenly bodies. (NASA, Trans.). Washington
- Jezewski, D.J, & Mittleman, D. (1982). An analytic approach to two-fixed-impulse transfers between Keplerian orbits. *Journal of Guidance, Control, and Dynamics*, 5(5), 458-464.
- Jin, H. & Melton, R. (1991). Transfers between circular orbits using fixed impulses. In *Spaceflight mechanics. Proceedings of the 1st AAS/AIAA Annual Spaceflight Mechanics Meeting*, Houston, TX, Feb. 11-13, 1991. Pt. 2 (A93-17901 05-13), p. 833-842.
- Sgubini, S, & Teofilatto, P. (2002). *Optimal Impulsive Maneuvers in Orbital Transfers*. Unpublished paper presented at 5th Cranfield DCSSS Conference, King's College, Cambridge, UK
- Soop, E.M. (2010). *Handbook of geostationary orbits*. Torrance, CA: Microcosm, Inc. and Dordrecht, The Netherlands: Kluwer Academic Publishers.
- Vallado, D. A. *Fundamentals of astrodynamics and applications*. Hawthorne, CA: Microcosm Press and New York, NY: Springer
- Wertz, J.R, & Larson, W. J. (1999). *Space mission analysis and design*. Hawthorne, CA: Microcosm Press and New York, NY: Springer

Appendix A

Run A input file

Initial Semi Major Axis : 42086
Initial eccentricity : .000931444358
Initial inclination : .112549692
Initial raan : -.691284657
Initial arg of perigee : 3.138571101
Initial true anomaly : -0.182442757
Solar Radiation (Cp) : 1.25
Initial epoch year : 2012
Initial epoch month : 03
Initial epoch day : 28
Initial Epoch hour : 12
Initial Epoch minutes : 13
Initial epoch seconds : 31
Burn epoch year : 2012
Burn epoch month : 03
Burn epoch day : 29
Burn Epoch hour : 00
Burn Epoch minutes : 00
Burn epoch seconds : 00

Appendix B

Run A input file

Initial Semi Major Axis (km) : 42086
Initial eccentricity : .0009
Initial inclination (rad) : .1
Initial raan (rad) : -1
Initial arg of perigee (rad) : 0
Initial true anomaly (rad) : 0
Solar Radiation (Cp) : 1.25
Initial epoch year : 2013
Initial epoch month : 04
Initial epoch day : 26
Initial Epoch hour : 00
Initial Epoch minutes : 00
Initial epoch seconds : 00
Burn epoch year : 2013
Burn epoch month : 04
Burn epoch day : 27
Burn Epoch hour : 01
Burn Epoch minutes : 00
Burn epoch seconds : 00
Desired Final Longitude (deg) : 90

